

Feasibility Study of a FNAL Booster's 2-nd Harmonic Cavity

G. Romanov and I. Terechkine

Introduction.

The addition of second harmonic RF cavities to the Fermilab Booster's accelerating system promises improvement of injection efficiency and increased power of the beam [1], which favors many projects. As the main frequency in the Booster changes from 37.87 to 52.82 MHz, the required frequency range in the second harmonic cavities is from 75.74 MHz to 105.64 MHz. This tuning range exceeds what was achieved in the tunable RF cavities that were designed and built in LANL, studied at SSC and FNAL, and tested in the pulsed mode at TRIUMF [2, 3]. Therefore designing and prototyping a device tunable within this range requires substantial RF, magnetic, and thermal studies.

Fig. 1 shows one of studied scenarios of the frequency ramp accompanied with the timing of the accelerating voltage in the second harmonic cavities [4]. For this particular scenario, a 100 kV accelerating voltage is used in the time intervals $0 < t < 3$ ms and 16 ms $< t < 19$ ms.

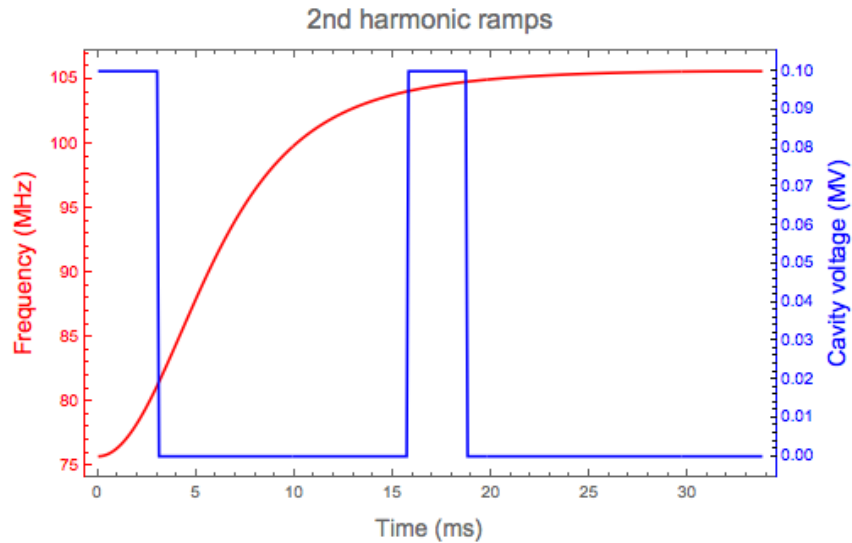


Fig. 1. Frequency ramp and the accelerating voltage in the 2-nd harmonic cavities

Similar to the technical solution used in [3] and [4], transversely biased Yttrium Iron Garnet (YIG) material must be used in a tuner of the second harmonic Booster cavity to keep the RF power loss manageable. For the current version of the cavity design, AL800 gyrotropic material from TRAK Ceramics, Inc. was chosen. Studies of the material properties of this material are summarized in [5], [6], and [7]. Static magnetic properties of the material control the level of the magnetic field, which, in turn, define the loss tangent. Static magnetization curve found in [6] is shown in Table 1 below.

Table 1: Tabulated static magnetization curve of AL800 garnet material.

H (Oe)	0	1.33	2.36	2.76	3.85	6.00	10.00	17.5	37.5	61.54	94.44	145.16	343.75
B (G)	0	200	350	400	500	600	650	700	750	800	850	900	1100
μ	150	150	148	145	130	100	65	40	20	13	9	6.2	3.2

In [5] it was shown that the loss tangent of the AL800 material can be found by using a constant loss coefficient $\alpha \approx 0.0033$ in the classical expression [8]:

$$tg(\delta_M) = \frac{\mu''}{\mu'} = \frac{\alpha\omega\omega_M(\omega_0^2 + \omega^2)}{(\omega_0^2 - \omega^2) \cdot (\omega_0^2 - \omega^2 + \omega_M\omega_0)} .$$

After relevant properties of the AL800 material were found, it became possible to take closer look at other aspects of the system design. The task of the heat removal out of the garnet material of the tuner seems to remain the most challenging to us. An option of using BeO disks (as was done in [2] and [3]) was ruled out due to safety concerns, and an attempt of using alumina cooling disks instead was made. This attempt combined precise 3D RF modeling and rough estimate of the thermal problem; the results gave rise to some optimism, which demanded more precise approach that would take into account fine details of the RF power loss distribution in the AL-800 blocks during frequency ramp. This note describes this stage of the study.

Geometry

Making 3D time-dependent multi-physics modeling is prohibitively time-consuming task; a 2D modeling approach was used instead. The only feature that differ this model from the 3D version is the absence of the power coupler and the amplifier. This results in some shift of the resonance frequency, which needs to be kept in mind. The geometry is shown in Fig. 2.

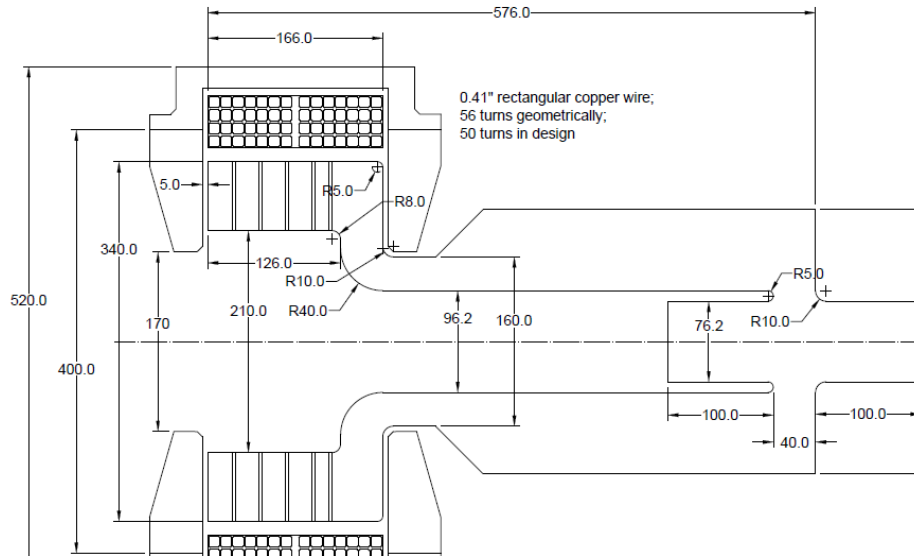


Fig. 2. 2D version of the RF design.

As in the 3D version of the design, to handle the heat deposited in the tuning section of the device, filled with gyrotropic material, its volume is subdivided into several sections (blocks) separated by alumina discs that are introduced to help in removing the heat. Thicknesses of the AL-800 blocks differs: starting from the tuner end of the cavity, they are 23.5 mm, 22 mm, 22 mm, 22 mm, and 13.5 mm. Thickness of each alumina disk is 3 mm. The bias coil is wound using 0.41" rectangular copper wire with a 0.2" diameter channel for water cooling; the number of turns in the coil is 50. The flux return must allow operation at frequencies up to ~50 Hz, so a solid ferrite pole is used to improve uniformity in the tuner area and a flux return is assembled using blocks of thin silicon steel profiles.

Tuning curve of the device in Fig. 2 is shown in Fig. 3. Here the resonant frequency of the cavity f is shown as a function of the ampere-turns in the bias coil Iw and compared with the polynomial approximation:

$$Iw(f) = 5.2 + 0.135 \cdot (f - 65) + 0.002 \cdot (f - 65)^2 - 1.1 \cdot 10^{-4} \cdot (f - 65)^3 + 4.6 \cdot 10^{-6} \cdot (f - 65)^4 \quad /1/$$

where the frequency is in MHz and the ampere-turns in kA. Using analytical approximation simplifies the final stage of this study when the procedure of the time averaging is applied.

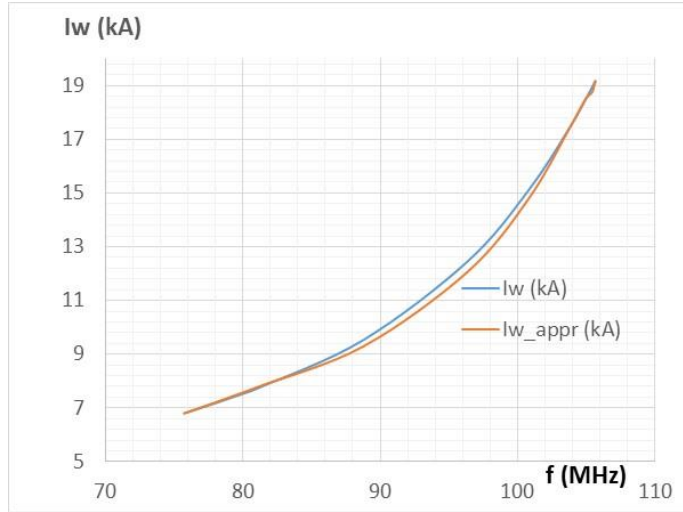


Fig. 3. Tuning curve of the cavity.

Static RF power loss

RF modeling of the 2D system was made using COMSOL RF modeling tool in the eigenvalue mode. Fig. 4 illustrates the case when the bias current $Iw = 6$ kA. At this low bias, the maximum value of permeability in the top garnet block in the figure (in Fig. 2 it is 13.5 mm thick block) is ~ 23 ; this results in a very high density of the RF power loss in this area.

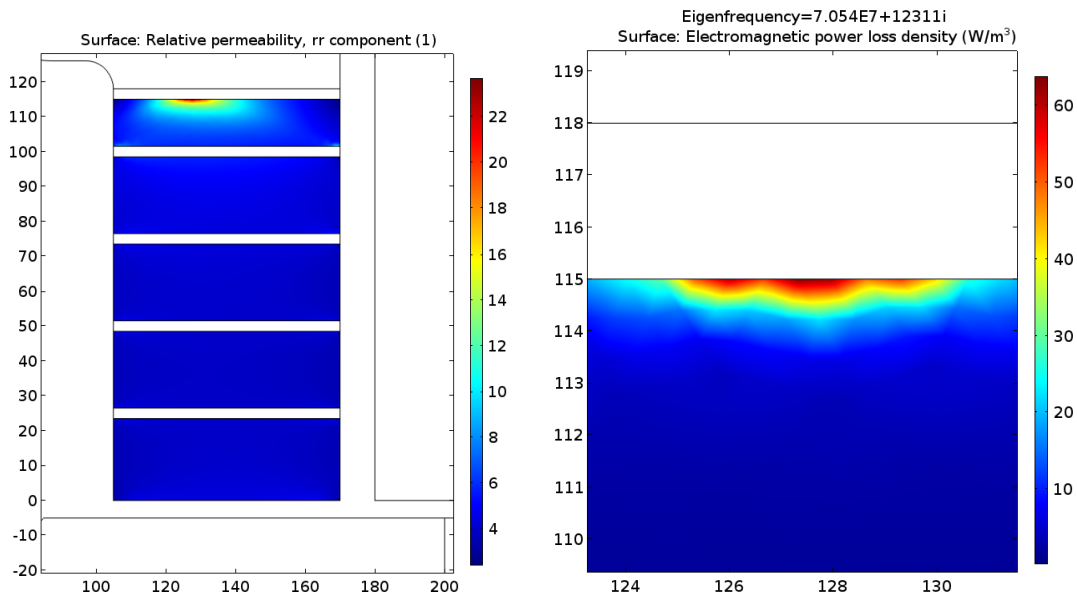


Fig. 4. Permeability and the power loss density in the top block at $Iw = 6$ kA.

The values of the RF power loss density, shown in the figure for the top part of the top block, must be re-scaled to the 100 kV accelerating voltage across the cavity gap; scaling coefficient k_w is the squared ratio of the required gap voltage (100 kV) to that furnished by the eigenvalue solver. The scaling gives the maximum power density in the hot spot $p_{max} = 600 \text{ W/cm}^3$. The hot spot has the longitudinal dimension (along the beamline) $\sim 1 \text{ mm}$ and the radial dimension $\sim 5 \text{ mm}$. When the bias current increases, as required by the frequency ramp pattern in Fig. 1 and the tuning curve in Fig. 3, the power loss density in the hot spot becomes much less pronounced and finally disappears. To properly understand expected temperature rise in the garnet material, this change of the spatial distribution of the RF power loss must be taken into account during time averaging of the power loss density.

To understand the scope of thermal problem, average power loss in the whole tuner, both in the garnet and in the ceramic disks, was calculated first.

Table 2 summarizes results of static modeling for several sets of the bias current I_w . In this table P_{mag} is the magnetic losses in the garnet, $P_{e/m}$ is the sum of magnetic and electric losses in the garnet, and P_{tot} includes the (electric) power loss in the alumina cooling disks.

Table 2. Static RF power loss in the tuner

I (kA)	6.00	6.25	6.5	6.75	7.0	7.5	8	9	11	15	20	25
f (MHz)	70.54	72.46	74.23	75.88	77.40	80.11	82.51	86.54	92.76	100.96	106.71	110.43
$k_w \cdot 10^{-6}$	9.352	9.253	9.159	9.069	8.985	8.832	8.693	8.456	8.079	7.577	7.226	7.001
P_{mag} (W)	43926	39732	36689	34128	31917	28218	25184	20491	14141	7618	4302	2696
$P_{e/m}$ (W)	51945	47865	44893	42366	40167	36456	33370	28508	21664	14273	10225	8111
P_{tot} (W)	53115	49052	46079	43554	41353	37635	34537	29647	22730	15215	11065	8880
Q	2865	3229	3545	3845	4006	4255	4757	5717	7325	10226	13615	16012

The total heating power P_{tot} in Table 2 can be approximated by an analytical function of the current:

$$P_{tot} \text{ (W)} = 481162 \cdot (I_w)^{-1.258} \quad /2/$$

Graphs in Fig. 5 compare results of modeling with this analytical approximation.

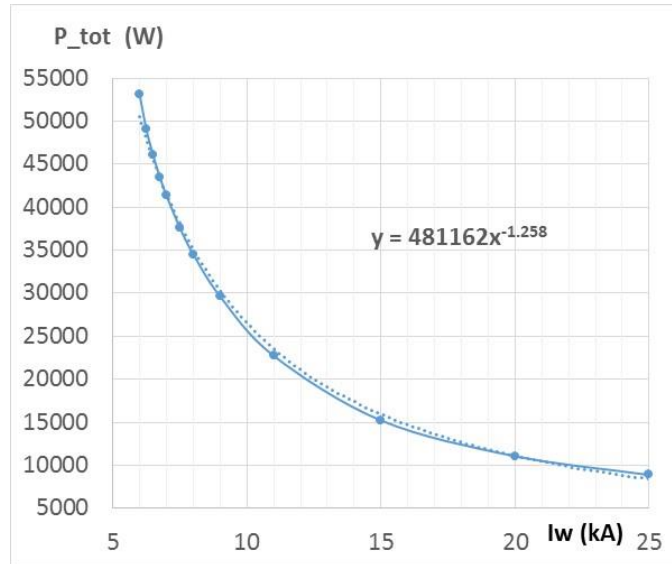


Fig. 5. Static power loss in the tuner as a function of the bias current.

Time-averaged power loss

To get time-averaged power loss in the tuner, we will use the following analytical approximation of the required frequency ramp shown in in Fig. 1:

$$\text{For } 0 < t < 3 \text{ ms} \quad f \text{ (MHz)} = 75.7316 - 0.0466 \cdot t + 0.7774 \cdot t^2 - 0.0513 \cdot t^3 \quad /3a/$$

$$\text{For } 3 \text{ ms} < t < 25 \text{ ms} \quad f \text{ (MHz)} = 65.3 + 6.47 \cdot t - 0.415 \cdot t^2 + 0.0128 \cdot t^3 - 0.00018 \cdot t^4 + 8.3 \cdot 10^{-7} \cdot t^5 \quad /3b/$$

Graphs in Fig. 6 compare the required frequency ramp with its analytical approximation.

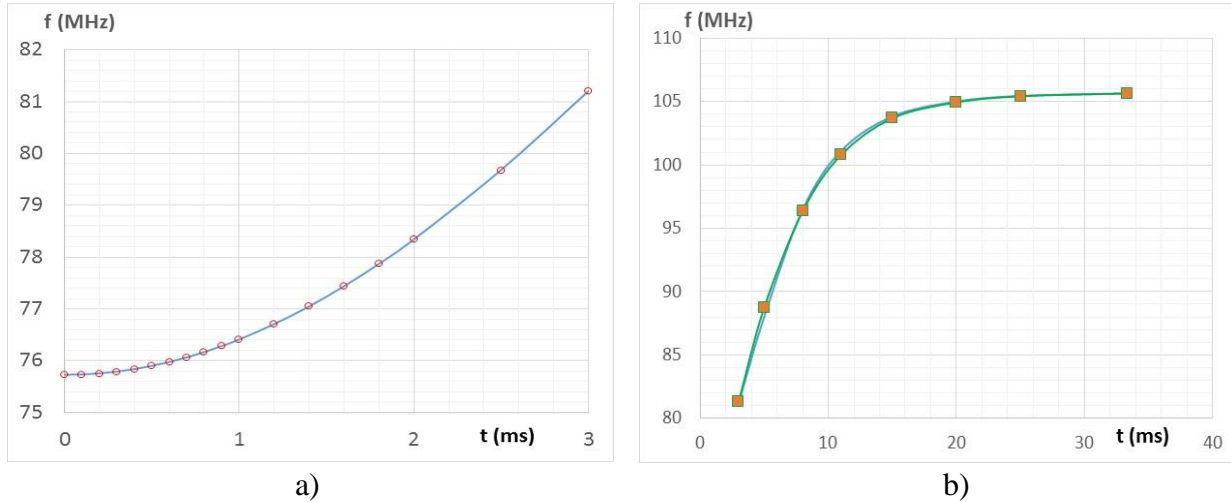


Fig. 6. Required frequency ramp and its analytical approximation: a) $t < 3$ ms; b) $t > 3$ ms.

The following procedure was used for the time averaging of the RF power losses:

- Using expressions /3/, frequency is found for each time step between $t = 0$ and $t = 33.3$ ms. Time increment of 0.5 ms provides adequate precision for the initial part of the ramp.
- Using expression /1/, bias current is found for each frequency in the sequence.
- Using expression /2/, the RF loss power is found for each time step.
- Sum of the heat deposited at each step, while taking into account the profile of the accelerating voltage in Fig. 1, gives the energy deposited in the tuner in one cycle.
- Applying the required operation frequency (15 Hz) one gets the time-averaged power deposited in the tuner.

As a result of implementation of this procedure, the average power in the tuner is found to be ~ 3560 W, which is about an order of magnitude lower than the static loss found earlier. Since removing this power seems manageable task, we can make another step forward and find the impact of very non-uniform spatial distribution of the losses in the top (as shown in Fig. 4) garnet block.

Power consumption in the “top” garnet block

The problem was addressed similar to how it was solved for the whole tuner with the only exception that the top block of the garnet material was subdivided into several areas where the space-averaged power loss density was extracted at several settings of the excitation current. For each area, an interpolation formula was suggested to calculate the power loss density at any

current. Using spatially-averaged density of the RF power loss instead of taking into account fine structure of the non-uniform power loss in the material significantly simplifies the process of time averaging. Similar to what was done earlier, time stepping was applied, and the time- and space-averaged power loss density was found for each area. For higher accuracy, in the areas with non-uniform distribution of heating, the number of subdivisions must be sufficiently high. In our case, we've chosen to have just eight areas; smaller area sizes are used where the non-uniformity is stronger. The cross-section of the block is divided by straight lines into four columns and two rows; Fig. 9 below can help to visualize the chosen way to sub-divide the block. Each area has been indexed: the first index is the number of the row from the top and the second index is the number of the column from the center.

Table 3 summarizes result of calculating spatially averaged static heat deposition density p_{nm} in eight areas of the top block for several settings of the bias current I_w .

Table 3. Spatially-averaged heat deposition density in the top garnet block (in W/cm^3)

I_w (kA)	$p11$	$p12$	$p13$	$p14$	$p21$	$p22$	$p23$	$p24$
6.7	12.85	18.76	9.03	3.82	11.08	9.41	7.09	4.52
6.8	12.26	17.08	8.59	3.78	10.81	9.13	6.88	4.42
7.5	9.91	10.41	6.62	3.52	9.27	7.62	5.76	3.89
8.5	8.1	7.16	5.11	3.18	7.75	6.15	4.69	3.34
10	6.73	5.28	3.98	2.81	6.52	5.01	3.86	2.87
12	5.58	4.17	3.2	2.37	5.39	4.07	3.14	2.38
15	4.98	3.61	2.78	2.12	4.72	3.49	2.7	2.09
19	4.33	3.08	2.37	1.85	4.06	2.97	2.3	1.8

For each column in the table, interpolation function is found; graphs in the figures below compare original sets of the data with corresponding analytical approximation.

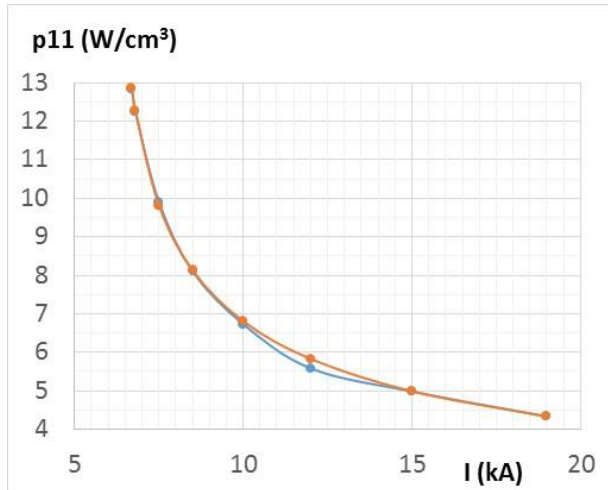


Fig. 711: $p_{11} (W/cm^3) = 11.8 \cdot (I_w - 5.9)^{-0.39}$

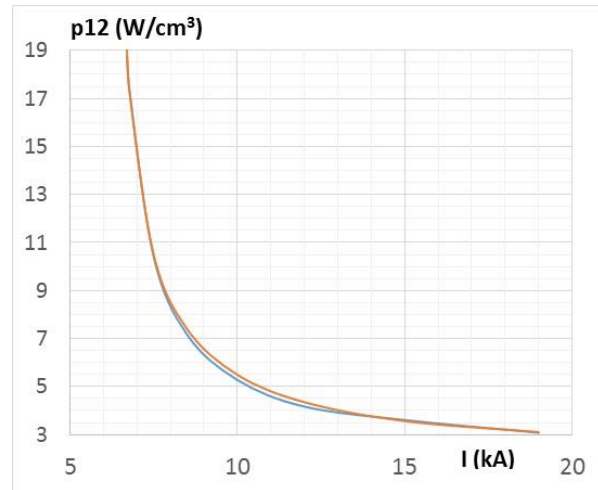


Fig. 712: $p_{12} (W/cm^3) = 12.3 \cdot (I_w - 6.2)^{-0.63} + 0.05 \cdot (I_w - 6.2)$

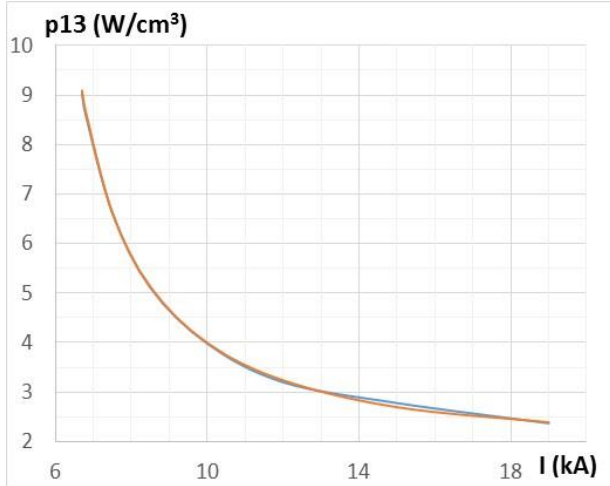


Fig. 7₁₃: $p_{13} \text{ (W/cm}^3\text{)} = 11.5 \cdot (I - 5.3)^{-0.72} + 0.047 \cdot (I - 5.3)$

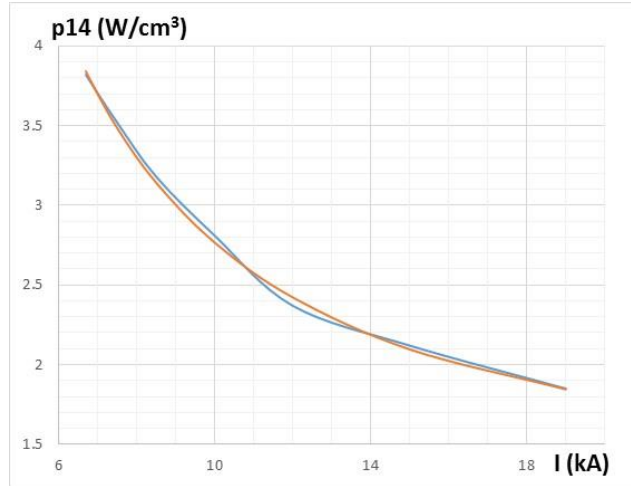


Fig. 7₁₄: $p_{14} \text{ (W/cm}^3\text{)} = 15 \cdot (I - 1)^{-0.8} + 0.02 \cdot (I - 1)$

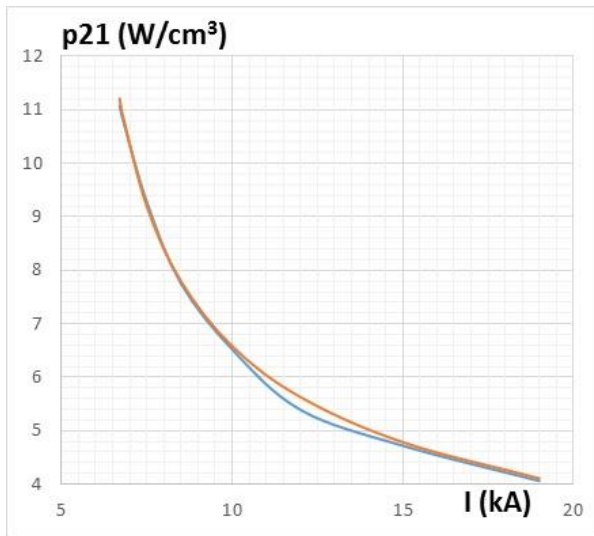


Fig. 7₂₁: $p_{21} \text{ (W/cm}^3\text{)} = 13 \cdot (I - 5.3)^{-0.44}$

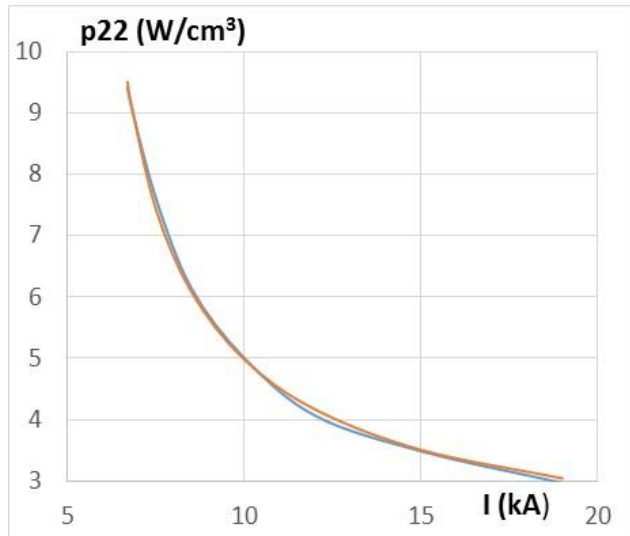


Fig. 7₂₂: $p_{22} \text{ (W/cm}^3\text{)} = 11.4 \cdot (I - 5.3)^{-0.55} + 0.025 \cdot (I - 5.3)$

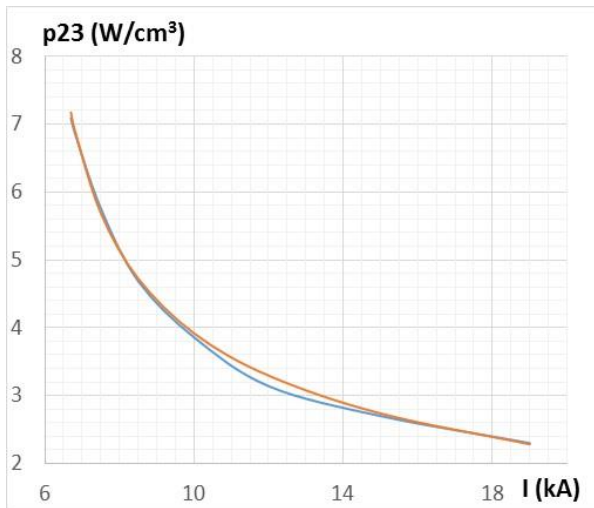


Fig. 7₂₃: $p_{23} \text{ (W/cm}^3\text{)} = 7.8 \cdot (I - 5.5)^{-0.45} - 0.01 \cdot (I - 5.5)$

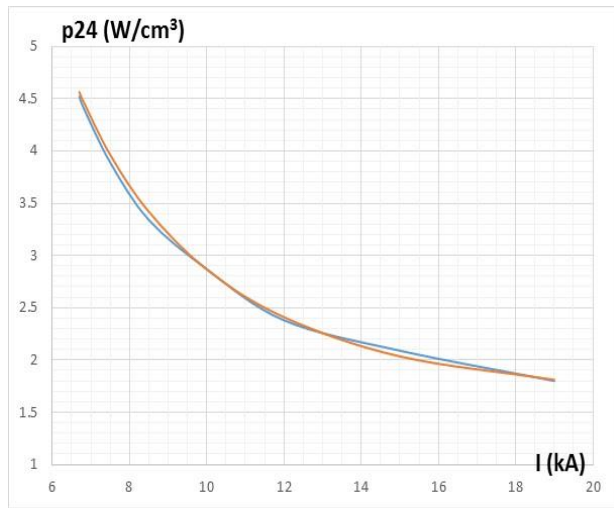


Fig. 7₂₄: $p_{24} \text{ (W/cm}^3\text{)} = 35 \cdot (I - 1.0)^{-1.2} + 0.04 \cdot (I - 1.0)$

The procedure for time averaging of the power loss density closely follows the one used earlier for the power loss in the tuner with the three last steps modified as the following:

- For each time step for each area of the top block, spatially averaged RF power loss density is found using interpolation formulas in Fig. 7.
- For each area of the top block, sum of spatially averaged heat density deposited at each time step gives the spatially averaged energy density in one cycle.
- Applying the required operation frequency (15 Hz), one gets the time- and space-averaged power loss density in each of eight areas of the top block.

Results of implementation of this procedure are summarized in Table 4, where w is the spatially averaged energy density per cycle, p is the time and spatially average power density, V is the volume of corresponding area, and P is the power deposited in the area.

Table 4. Summary of the time and spatial energy density calculation

	Area 11	Area 12	Area 13	Area 14	Area 21	Area 22	Area 23	Area 24
w (J/cm ³)	0.058	0.064	0.037	0.02	0.053	0.042	0.032	0.022
p (W/cm ³)	0.867	0.961	0.562	0.307	0.794	0.637	0.483	0.336
V (cm ³)	62.5	61.3	68.3	88.7	106	104	116	151
P (W)	54.2	58.9	38.4	27.3	84.2	66.2	56.0	50.8

The total time-averaged power deposition in the 1-st block is found by summing the last row of the table: $P_{top} = 436$ W. Calculation of the averaged power deposited in the top block using the same algorithm gives the same result.

Power consumption in the alumina disks surrounding the top garnet block

To switch to solving thermal problem, we need to find the time-averaged power loss density in the alumina disks. Table 5 summarizes results of calculation of the power deposited in each disk (top and bottom) at several current settings.

Table 5. Power deposition in the ceramic discs

I_w (kA)	6.7	6.8	7.6	8.5	10	12	15	19
P_{top} (W)	450	449	440	425	403	358	342	312
P_{bott} (W)	360	359	357	351	337	301	288	262

Thickness of each disk is 3 mm; because the power loss is purely electrical, at each bias current setting, the RF loss power density is a one-dimensional function of the radius. Moreover, it appears that only the amplitude of this function changes with the current setting; the shape of the distribution remains the same. As a result, to calculate the power loss in the disks at any current, we can use the following approximations function:

$$\text{For the top disk,} \quad p = A_{top}/r^{2.6}. \quad /4a/$$

$$\text{For the bottom disk} \quad p = A_{bott}/r^{2.2}. \quad /4b/$$

At each bias current, coefficients A_{top} and A_{bott} are found by normalizing to the measured power loss. The following expression for the coefficients are obtained:

$$\text{For the top disk,} \quad A_{top} = 5.18 \cdot P_{top} [\text{W}/\text{cm}^{0.4}]. \quad /5a/$$

$$\text{For the bottom disk,} \quad A_{bott} = 1.85 \cdot P_{bott} [\text{W}/\text{cm}^{0.8}]. \quad /5b/$$

Graphs in Fig. 8 below show how the coefficients A for the top and the bottom disks change with the bias current. Also shown are interpolating polynomials $A_{top}(Iw)$ and $A_{bott}(Iw)$, which are made linear and mostly exceeding the calculated values (providing an additional safety reserve):

For the top disk: $A_{top}(Iw) = 2250 - 60 \cdot (Iw - 8)$ /6a/
 For the bottom disk: $A_{bott}(Iw) = 650 - 15 \cdot (Iw - 8)$ /6b/

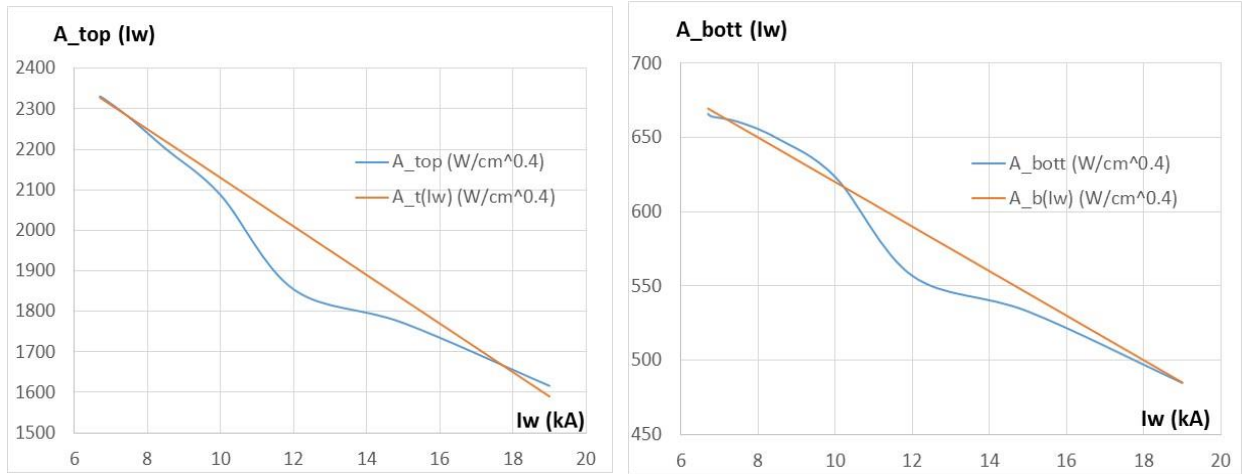


Fig. 8. Coefficients A in /4/ and /5/ as functions of the bias current.

Using these functions and the procedure of the time averaging described (and used twice) earlier, we can find the time-averaged coefficients A:

For the top disk, $A_{top_av} = 220.5 \text{ W/cm}^{0.4}$. /7a/
 For the bottom disk, $A_{bott_av} = 65.0 \text{ W/cm}^{0.8}$. /7b/

So, in the top disk, the power loss density is

$$p_{top} (\text{W/cm}^3) = 220.6/r^{2.6}. \quad /8a/$$

For the bottom disk,

$$p_{bott} (\text{W/cm}^3) = 65/r^{2.2}. \quad /8b/$$

Integration through the volume of the disks gives the average power deposition 42.5 W in the top plate and 35.1 W in the bottom plate.

Thermal problem solved

Knowing RF power loss density in all elements of the top block of the tuner, we can set thermal problem. Insulating boundary conditions were used for the top surface of the top Al_2O_3 disk and for the middle of the bottom Al_2O_3 disk. Two-millimeter stainless steel wall were used to separate the elements from the constant temperature boundary condition on the inner and outer radial borders. The following data for the thermal conductance were used:

- for the 95% Al_2O_3 disks $k = 26 \text{ W/(m}\cdot\text{K)}$;
- for the Al-800 garnet material, $k = 3.5 \text{ W/(m}\cdot\text{K)}$;
- for the stainless steel, $k = 15 \text{ W/(m}\cdot\text{K)}$.

Fig. 9 shows the map of the RF power loss density in the elements of the model. In Fig. 10 temperature rise corresponding to this power loss density is shown. The maximum temperature rise in the middle of the top block is 35°C.

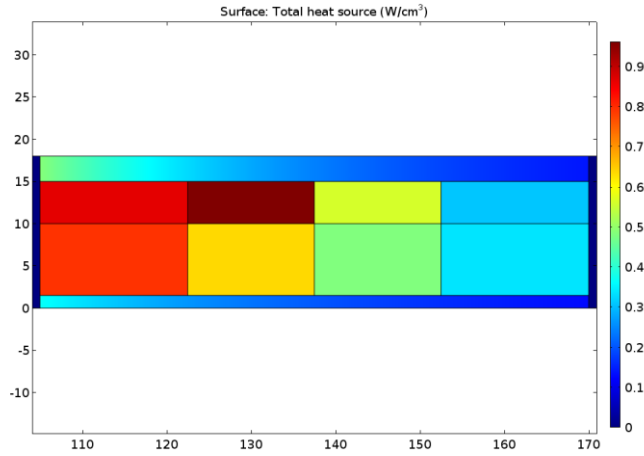


Fig. 9. Assumed time averaged RF power loss density in the thermal model (W/cm^3).

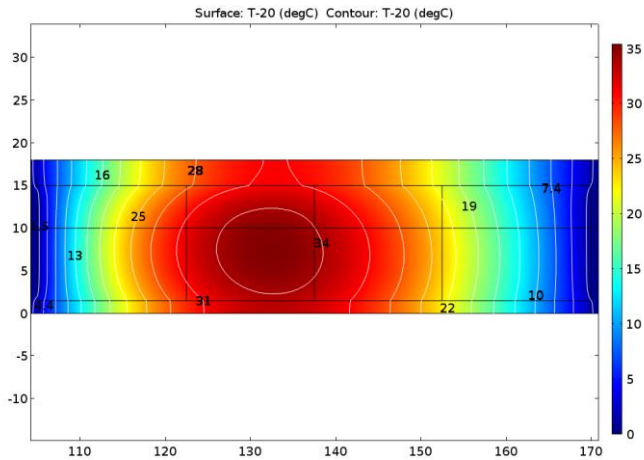


Fig. 10. Temperature map in the top disk of the RF tuner.

Summary

A study was made to understand the impact of highly non-uniform distribution of the heating RF power in the garnet material of the 2-nd harmonic cavity RF tuner. The last (August 2015) version of the cavity design RF frequency ramp and accelerating amplitude was used, and the time-averaged power deposition in the top garnet block and separating ceramic disks were found. This data was used as an input into a thermal problem; the expected temperature rise in the garnet material is well below of what was expected when a conservative approach was used. This provides an opportunity for further optimization of the device with the goal to minimize the maximum bias current and improve the uniformity of the magnetic field inside the garnet material.

It worth to mention that the current RF design can be further optimized if all tuner (not only its top portion) is analyzed using the described method.

It seems mandatory starting iterations on a design concept that would address thermal interfaces problem. These interfaces were accepted ideal in this study, but in reality this can be another major problem to solve.

References:

- [1] G. Romanov, et al, “Perpendicular Biased Ferrite Tuned Cavities for the Fermilab Booster”, IPAC-14, Dresden, Germany, 2014.
- [2] W. R. Smythe, et al, “RF Cavities with Transversely Biased Ferrite Tuning”, IEEE Trans. On Nuclear Science, NS-32, no. 5, October 1985.
- [3] R. L. Poirier, et al, “A Perpendicular AC Biased Ferrite Tuned Cavity for the TRIUMF Kaon Factory Booster Synchrotron”, EPAC 1990, proc., pp. 988 – 990.
- [4] Y. Tan, private communication
- [5] R. Madrak, et al, “Static Permeability of AL-800 Garnet Material”, FNAL TD note TD-15-004, April 2015.
- [6] R. Madrak, et al, “Loss Tangent of AL-800 Garnet Material”, FNAL TD note TD-15-005, June 2015.
- [7] R. Madrak, et al, “Permeability of AL800 Garnet Material”, FNAL TD note TD-15-014, July 2015.
- [8] D. M. Poser, Microwave Engineering, John Wiley & Sons, Inc., 1998.